Posted: May 1, 2025

A Prototypical Design of a Passive Magnetic Suspension System

Zimo Chen[1]

[1]Byron College; ORCID: 0009-0001-7677-0306

Abstract

Suspension systems are continuously developed in the field of engineering to reduce mechanical vibrations. They are used to isolate delicate systems from vibrations to allow proper functioning and prevent damage. This article proposes an alternative suspension mechanism employing the repulsion forces between magnets with eddy current damping combined with air damping. No sealing is required in this system, so there is no risk of leakage. Calculations have been done to describe the damping characteristics of this suspension system. Static and dynamic tests are done on a prototype to justify the feasibility of this mechanism, obtaining a force-distance graph and transmissibility characteristics. Results suggest that this suspension system is very progressive compared to conventional suspension systems, but it provides a satisfying vibration reduction performance. The Magnetic Suspension System allows non-direct contact from the source of vibration to the detection end, providing rapid responses to shock. The Magnetic Suspension System is also not subjected to metal fatigue and is highly unlikely to undergo sudden failure.

Keywords: magnetic repulsion; suspension system; eddy current damping; prototype

1 Introduction

The suspension system is a vital part of a modern vehicle and many industries. It is used to isolate vibrations and shocks or reduce their impact on other components. They can often be found on cars and bikes where they isolate the vehicle from vibrations on the tyres, improving comfort and controllability. For off-road or high-speed applications, the suspension system also keeps the tyres constantly in contact with the ground surface, giving maximum traction and allowing the best acceleration, braking, and cornering performance [1]. They are also used in the aerospace industry, for example, a soft suspension system is used on the James Webb Space Telescope (JWST) to isolate the optic components from high-frequency vibrations due to the operation of other components, such as the Reaction Wheel Assembly and the cryocooler [2]. At the most basic level, a suspension system must include two parts: a spring and a damper. In the case of a car landing from a jump, the spring extends the time for deceleration and reduces the peak force on the frame of the car. During this process, the spring converts the kinetic energy of the car into

elastic potential energy. However, if not enough energy is dissipated, the potential energy would be released after the shock and push the car off the ground again as a result of the conservation of energy. The shock absorber prevents this from happening through various damping mechanisms. It absorbs excess energy released from the spring and often converts it into the internal energy of the damping fluid or air.

This design of a magnetic suspension system is a prototypical attempt without any specific aim of use. It is a passive suspension system that uses the repulsion force between the magnets as the spring, with damping achieved by a combination of eddy current and air damping.

2 Design Overview

The Magnetic Suspension System (MSS), shown in fig. 1 consists of five main components: Shell, Bottom, Piston, Top and Neodymium magnets. The full technical drawing can be found in the appendix. All components apart from the magnets and the cushioning parts are made of Aluminium 6061 alloy. To ensure smooth sliding motion between the piston and the shell, the shell and the piston are set to an H8/c7 [1] clearance fit. Similarly, the piston's inner hole and the central rod are set to an H11/c11 clearance fit (ISO-286). This MSS can be connected to some external machines with M10 and M8 fasteners on the bottom and the top. The maximum travel of this device is 77 mm. Rubber cushions are added to prevent direct impact between the magnets that may cause the magnets to shatter. Nitrile rubber is used specifically due to its good mechanical performance and high oil resistance, which allows it to function properly in the presence of lubricating oil. The device can be manufactured mainly by lathe work, with some other processing for the connection features on components "Bottom" and "Top". This prototype was made by a manufacturer based in China.

3 Spring

Generally, springs can be categorised into three general types based on the relationship between the force applied to a spring and the displacement: linear springs, variable rate springs and constant springs [3]. A linear spring has a constant spring rate and follows Hooke's law, where the deformation of a spring is directly proportional to the force applied to deform it. This relationship can be described using $F = kx$, where F is the force applied, x is the displacement and k is the spring constant. Variable rate springs have multiple or changing spring rates. For example, an air spring's spring rate increases along with the displacement as the pressure is inversely proportional to the volume of the air. A constant spring requires an approximately constant force no matter the displacement, which makes it suitable for counterbalancing heavy loads yet not common in suspensions [3].

Theoretically, the force between two magnetic monopoles can be described using the formula

$$F = \frac{\mu m_1 m_2}{4\pi r^2} \tag{1}$$

where μ is the permeability of the intervening medium, m_1 and m_2 are the magnetic pole

[1] By ISO-286 standard. Specific values can be found in *Appendix II. Technical drawing of the Magnetic Suspension System prototype*

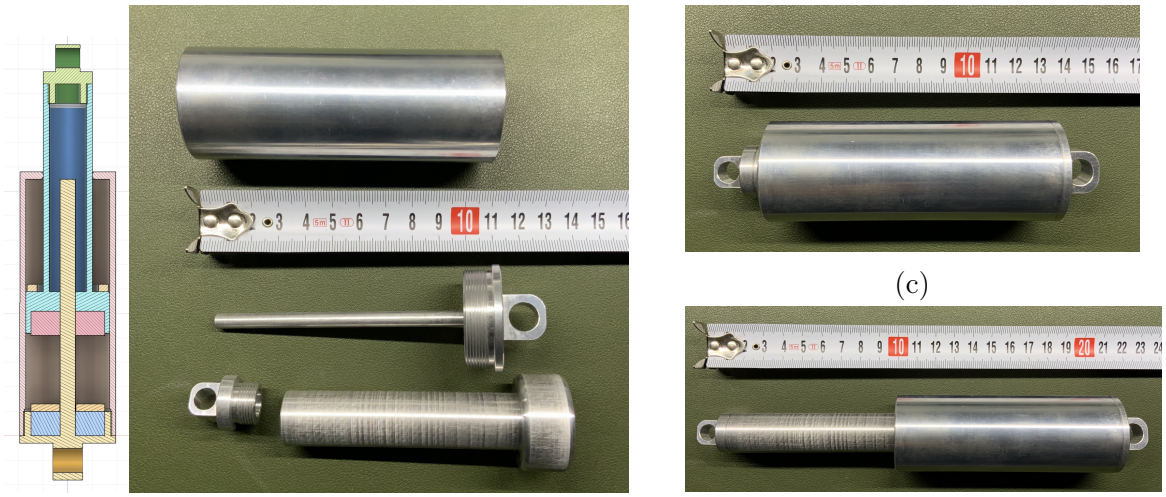

(a) (b) (c) (d)

Figure 1: (a) the cross-sectional profile of the device; (b) components disassembled; (c) the MSS at its minimum length; (d) the MSS at its maximum length.

strengths, and r is the distance between the two poles. However, the force between two magnets is difficult to calculate as each magnet is a summation of multi-trillion-trillion mini magnetic dipoles, each interacting with another multi-trillion-trillion mini magnetic dipoles of the other magnet. For practical purposes, the magnetic repulsion force was determined experimentally during the design of this suspension system.

A linear translational testing frame is designed to accurately control the distance between the two magnets accurately when measuring the force between the magnets. The apparatus (fig. 2) consists of 3 units, i.e. fixture, control and slider, and in total, 14 components. The fixture unit contains 7 components and ensures a strong connection with the stand. Three M6 screws are used to bind the frame with the stand. Two of the screws are placed horizontally and they do not point at the centre of the pole. Instead, they are set at an angle to oppose any force couple along the rod. The control unit allows precise adjustments of the distance between the two magnets. Employing a worm shaft and worm gear structure, minimal force is required to control the spacing as a result of the 16:1 mechanical advantage. In addition, the self-locking nature of the worm shaft and gear structure facilitates measuring the distance between the magnets. The L-shaped slider is joined to the large worm gear by a rack on its side. Features were designed at the end of the slider for the convenience of experiments. An additional rib was added to reinforce the stiffness of the slider. All components are made using PLA by 3D printing apart from the bolts and nuts. However, the rack experienced significant elastic deformation under load, preventing the measurement of forces at smaller distances. This could have been solved by using an alternative material stronger than 3D-printed PLA. An aluminium rod is placed through the magnets to prevent them from rotating and, hence, aligning their polarity.

The dimensions of the neodymium ring magnet are N52 $\varnothing$ 30 $\times$ 5mm with a $\varnothing$ 6 mm hole in the middle. Multiple arrangements of the magnets are tested, for example, between a set of two magnets and another set of three magnets (denoted as 2-3). The force between the magnets is measured using a top pan balance, and the distance, x, between the faces of the magnets is measured using a ruler. An additional variable, "True distance", is introduced (denoted by x_{True}) to allow a better fitting model. It is calculated by adding x by half of

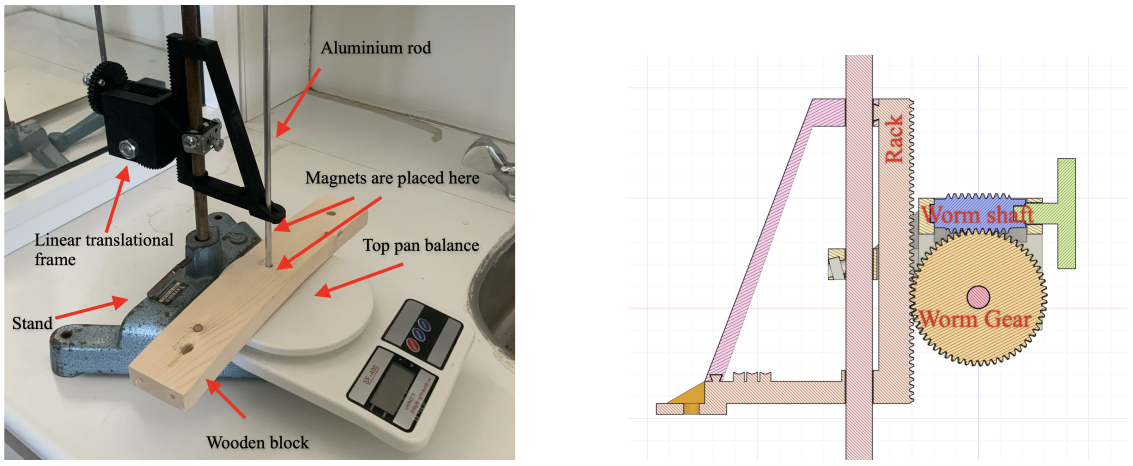

(a) (b)

Figure 2: (a) Photo of the apparatus. The rod goes through the wooden block to prevent it from sliding. The block has two contact points with the top pan balance, allowing more accurate readings on the balance. (b) cross-section drawing of the translational frame

the length of each set of magnets.

Shown in fig. 3, by plotting F against x_{True} in logarithmic scales, the data displays a decreasing linear pattern. One of the points in the series "2-3" (labelled with a hollow diamond) appears significantly away from the trend, suggesting an error during the experiment, and is therefore ignored when calculating the regression line. The values of the coefficient of determination (R^2) of the regression lines of all series are greater than 0.99, indicating strong linear correlations. The experiment suggests that the repulsion force and the distance between the magnets follow a power law with some negative exponent less than -2, i.e. $F = kx^n$, where $n \leq -2$ and the value of n is related to the arrangement of the magnets[2]. For example, the equation of the regression line under the logarithmic graph of set "2-4" is $\log_{10}(F) = 4.7257 - 2.8978 \log_{10}(x_{\text{True}})$, which converts to a force-distance curve with the equation $F = 53200 \cdot (x_{\text{True}})^{-2.8978}$.

The minor differences between the "3-3" and "2-4" series suggest that the arrangement of the magnets has little effect on the force curve when the total number of magnets remains constant. The same experiment is also done with two neodymium magnets with ⌀40 and the same thickness and hole diameter. A clear increase in the repulsion force is observed whilst following the same general formula (fig. 4); therefore, the diameter of the magnets is also a significant factor; magnets with greater diameter exert greater repulsion forces and can be used for applications where a stronger spring force is required.

The magnetic forces can be calculated using online calculators, for example, the K & J Magnetics Magnet Force Calculator [4].

Overall, the experiment suggests that a magnetic spring has a progressive spring rate with an n value less than -2. In comparison, a conventional air spring has an n value of -1 and is less progressive than a magnetic spring. The feature enhances comfort by providing a

[2]From all experiments conducted in this article and the literature found, no value of $n > -2$ is observed or recorded. However, this restriction is not strictly proved in this paper and no evidence that explicitly points out this constraint on the range of n is found.

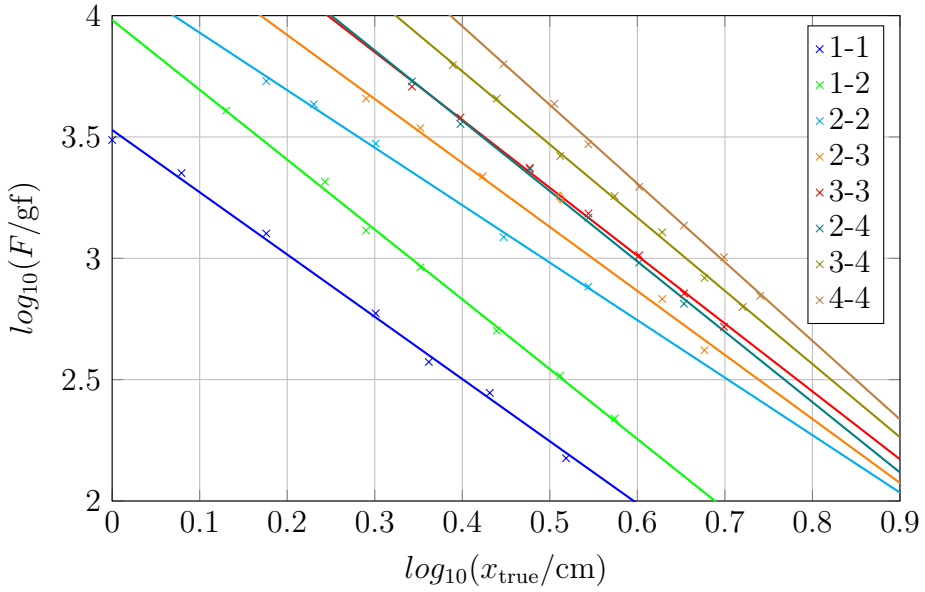

Figure 3: Repulsion force (F) vs the true distance between magnets(x_{True}). Dimension of magnets: N52 ⌀30 × 5 mm with a ⌀6 mm hole. The gradient of the fitted curves ranges from -2.57 to -3.24, with an approximate decreasing pattern as the number of magnets increases, e.g. -2.64 for 2-3 and -3.01 for 3-4. Full data can be found in the appendix.

soft and smooth response to vibration with small amplitude, but also preventing the entire travel from being used up, or "bottom out", when it is impacted with a strong shock. It is commented by mountain bikers that progressive springs are more agile and playful [5]. Compared to a linear spring, a very progressive spring can be used under a wider range of forces within a smaller volume, making a more compact design possible in portable devices, aerospace modules or other scenarios.

In practical use, this system has a long lifetime and requires minimal maintenance. As the magnets are not directly in contact with each other, they are not subjected to structural degradation or mechanical fatigue. Nevertheless, the permanent magnets might need to be replaced after a long period as they might partially demagnetise each other as the similar poles are forced together for a prolonged period, yet this demanetisation process are easily detectable and does not yield sudden failure. This period depends on various factors and can be extended by using permanent magnets with high coercivity, for example, high-grading neodymium and samarium-cobalt magnets, which are harder to demagnetise under strong external magnetic fields. Alternatively, electromagnets can be used as they do not degrade over time, with additional energy consumption being the trade-off. The strength of the electromagnet is adjustable by changing the current through the coil using programmable electronic devices, giving the potential to generate any desired force curve. It is also advised to keep the magnets under low temperature and, crucially, not close to their maximum operating temperature, where beyond this temperature, the magnets do not perform as well as they are designed [6]. For an N52 grade neodymium magnet, the maximum operating temperature is set at around 80 °C. The device is not expected to accumulate enough energy to reach the maximum operating temperature. The air in the chamber is constantly exchanging through the orifice with the environmental air, hence the heating effect on air due to damping is negligible. The kinetic energy of the magnets is transferred to the Aluminium shell, causing a temperature change of the shell as well.

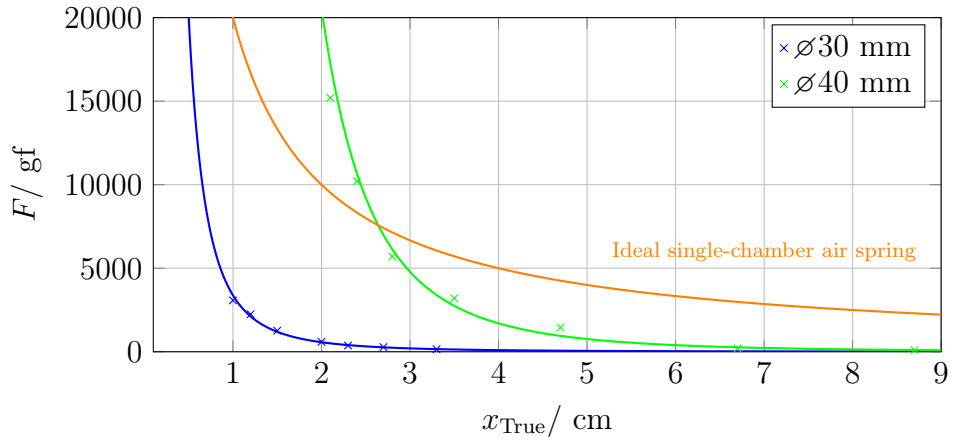

Figure 4: Repulsion force (F) vs the distance between magnets (x_{true}). Dimension of magnets: N52 ⌀30 × 5 mm with a ⌀6 mm hole, N52 ⌀40 × 5 mm with a ⌀6 mm hole . Full data can be found in the appendix.

However, since Aluminium has a relatively low specific heat capacity, it heats up and cools down rapidly and the energy can be transferred to the air in the chamber and discharged as well.

4 Damping

Damping is vital to a suspension system. Without appropriate damping, the spring would oscillate until all the energy is dissipated to the environment, causing instability and discomfort. For a conventional coil spring suspension system, the damping effect is often achieved by the resistance force when a piston with orifices travels through some viscous liquid (commonly oil). The damping force can be modified by adjusting the size of the orifice and changing to a damping oil of different viscosity. Unlike coil springs, air springs do not require additional dampers because it is, by nature, a good damping medium [7]. In this design, damping is achieved by applying Lenz's law and the resistance from discharging air from the chamber.

When a magnetic material is in relative motion with a conductor, eddy currents are induced in the conductor, which then induce a magnetic field which opposes the motion of the magnetic material. The kinetic energy of the piston is converted into electrical energy and later dissipated as heat due to the resistance of the conductor. This concept is maturely used in eddy current braking to slow down trains from high speed due to its wear-free advantage. In this design, an aluminium 6061 alloy shell is used because it is non-ferrous and is a good conductor of electricity. Aluminium 6061 alloy is also an economic metal alloy with multiple satisfying mechanical and chemical properties, including its high strength-to-weight ratio and its excellent corrosion resistance thanks to the aluminium oxide surface with high corrosion resistance. Unlike other common types of shock absorbers, Eddy Current Dampers (ECD) do not rely on fluids and do not require sealing, making them available for spatial applications. ECD is widely used in space flight and aircraft applications [8]. Furthermore, ECD is capable of converting the impact kinetic energy into electrical storage with a prototypical conversion efficiency of 2.33 % [9].

The quantity "magnetic friction force", F_{mf}, is introduced to describe the opposing force between a magnetic material and a conductor in relative motion. The magnetic friction

force can be deduced from Faraday's law and Joule's law of electric heating [10].

Let L be the length of a single wire in relative motion to a uniform magnetic field B in the y direction in time t. With Faraday's law, we have the induced electromotive force, ϵ, being proportional to the change of magnetic flux, Φ, where

$$\epsilon = -\frac{\mathrm{d}\Phi(B,t)}{\mathrm{d}t} = -BL\frac{\mathrm{d}y}{\mathrm{d}t} = -BLv \tag{2}$$

The power of heating in an electric conductor equals the current multiplied by the emf across the wire. The formula can be rewritten by substituting I by $\frac{\epsilon}{R}$.

$$P = IV = \frac{\epsilon^2}{R}. \tag{3}$$

In an ideal situation, the change of kinetic energy of the wire is equal to the change of internal energy of the wire. So, the power of heating due to the relative motion between the wire and the magnetic field is

$$P = \frac{\epsilon^2}{R} = \frac{(-BLv)^2}{R} = \frac{B^2L^2}{R}v^2, \tag{4}$$

and hence, the maximum magnitude of the magnetic friction force is

$$F_{mf} = \frac{P}{v} = \frac{B^2L^2}{R}v = bv, \tag{5}$$

where b is the coefficient of magnetic friction [10].

The effect is similar in practice with a piece of a magnet passing through an aluminium pipe, where the magnetic field around the magnet is not uniform. However, the formula suggests a good approximation where the damping force is directly proportional to the velocity of the piston and inversely proportional to the resistance of the shell and always opposes the direction of motion. In comparison with a conventional hydraulic damper, an EDC responds to shocks quicker and has a greater working range [11]. The damping effect, i.e. the gradient of a damping force-velocity graph, can be increased by using a thicker shell, a shell made of a material with less resistivity and the dimension and strength of the magnet. The arrangement of the magnets also affects the damping force. The magnets are often thin and arranged with alternating orientations to increase $\frac{\mathrm{d}\Phi}{\mathrm{d}y}$ and maximise the magnetic frictional force.

Apart from the damping effect from the eddy currents, air is also employed in the design as a damping element. The volume enclosed by the piston, the shell and the bottom cap is semi-sealed. The piston and the shell are in an H8/c7 clearance fit, and the piston and the central rod are in an H11/c11 clearance fit, which both allow some air to pass between the walls under a pressure difference as a side effect. The pressure difference also exerts force on the piston, where the magnitude of the force is dependent on the speed of the piston. If the damping force is too strong, one could add orifices on the shell that allow faster air discharge and, thus, less pressure inside the shell.

4.1 Preliminary calculation: force on the piston by the air pressure difference while exchanging air due to piston motion

This section attempts to describe the relationship between the velocity of the piston and the resistive force acting on the piston, i.e., a damping curve, via calculation. By the Ideal

Gas Law, the product of the volume of gas and the pressure of the gas is proportional to the amount of particles and the temperature of the gas, as

$$pV = nRT = \frac{m}{M_r} \cdot RT \tag{6}$$

$$p = \frac{m}{V} \cdot \frac{RT}{M_r} = \frac{m}{V} \cdot C \tag{7}$$

$$\text{with } C = \frac{RT}{M_r},$$

where:

p = pressure of gas, Pa,
V = volume of gas, m^3,
n = amount of gas particles, mol,
R = ideal gas constant, = $8.3144\,\mathrm{J\,K^{-}1\,mol^{-1}}$,
T = temperature of gas, K,
m = mass of gas, kg,
M_r = molar mass of gas, for atmospheric air $M_r = 28.965\,\mathrm{kg\,mol^{-1}}$.

The gas temperature is assumed to be constant as the air in the chamber continuously exchanges with the environment and can be approximated to be at room temperature.

Derive both sides with respect to time, t

$$\frac{\mathrm{d}p}{\mathrm{d}t} = \left(\frac{\frac{\mathrm{d}m}{\mathrm{d}t} \cdot v - m \cdot \frac{\mathrm{d}v}{\mathrm{d}t}}{v^2} \right) \cdot C \tag{8}$$

The gas pressure in the chamber is considered constant for each stroke, where the piston velocity is constant, because it massively simplifies the calculation process. Though this assumption is not entirely realistic in real-world applications, it gives a clue to the characteristics of air damping in the MSS. After all, this calculation is largely simplified under idealised conditions.

If p in the chamber is steady,

$$\frac{\mathrm{d}p}{\mathrm{d}t} = 0 \Longrightarrow \left(\frac{\frac{\mathrm{d}m}{\mathrm{d}t} \cdot v - m \cdot \frac{\mathrm{d}v}{\mathrm{d}t}}{v^2} \right) \cdot C = 0 \tag{9}$$

$$\frac{\mathrm{d}m}{\mathrm{d}t} \cdot v - m \cdot \frac{\mathrm{d}v}{\mathrm{d}t} = 0 \tag{10}$$

$$\frac{m}{V} = \frac{\frac{\mathrm{d}m}{\mathrm{d}t}}{\frac{\mathrm{d}V}{\mathrm{d}t}}. \tag{11}$$

Substitute eq. 7 into eq. 11, giving the steady pressure in the chamber

$$p = \frac{m}{V} \cdot C = \frac{\frac{\mathrm{d}m}{\mathrm{d}t}}{\frac{\mathrm{d}V}{\mathrm{d}t}} \cdot C = \frac{\frac{\mathrm{d}m}{\mathrm{d}t}}{A_p \cdot \frac{\mathrm{d}h}{\mathrm{d}t}} = \frac{q_m}{v_p} \cdot \frac{C}{A_p} = \frac{q_m}{v_p} \cdot k \tag{12}$$

$$\implies v_p = \frac{q_m \cdot k}{p} \tag{13}$$

$$\text{with } k = \frac{RT}{M_r A_p},$$

where:

q_m = discharge rate of gas, $\mathrm{kg\,s^{-1}}$
h = distance between the bottom and the piston, m,
v_p = velocity of the piston, $\mathrm{m\,s^{-1}}$,
A_p= area of the piston facing the air chamber, $\mathrm{m^2}$.

The rate of gas discharge through an orifice due to pressure difference under non-choked flow conditions is given by the formula [12],

$$q_m = C \cdot A_h \sqrt{2\ \rho_0\ p_1 \left(\frac{\gamma}{\gamma - 1}\right) \left[\left(\frac{p_2}{p_1}\right)^{\frac{2}{\gamma}} - \left(\frac{p_2}{p_1}\right)^{\frac{\gamma+1}{\gamma}} \right]} \tag{14}$$

and under choked flow conditions

$$q_m = A_h \sqrt{\gamma \rho_0 p_1 \left(\frac{2}{\gamma + 1}\right)^{\frac{\gamma+1}{\gamma-1}}} \tag{15}$$

Under choked flow conditions, the velocity of gas exiting the orifice is at sonic conditions. For ideal gases, this phenomenon happens when a critical pressure ratio between the upstream and downstream pressure is reached, where the critical pressure can be calculated from

$$\left(\frac{p_2}{p_1}\right)_{crit} = \left(\frac{2}{\gamma + 1}\right)^{\frac{\gamma}{\gamma-1}} \tag{16}$$

where:

C = orifice discharge ratio, dimensionless (assumed $C = 0.65$),
A_h = area of the orifice, $\mathrm{m^2}$,
ρ_0= density of gas, $\mathrm{kg\,m^{-3}}$,
p_1= upstream pressure, Pa,
γ= heat capacity ratio, dimensionless (approximated $\gamma = 1.4$ for air),
p_2= downstream pressure, Pa [12].

For air with $\gamma = 1.4$, $\left(\frac{p_2}{p_1}\right)_{crit} \approx 0.528$. During compression, air exits the chamber and enters the atmosphere, where the downstream pressure is assumed to be $p_2 = 101\,325\,\mathrm{Pa}$. Therefore, the airflow becomes choked when $p_{1(crit)} = 191\,800\,\mathrm{Pa}$. During rebound, $p_1 = 101\,325\,\mathrm{Pa}$, and $p_2 = 53\,530\,\mathrm{Pa}$.

Substituting eq. 14 to eq. 13 and eq. 15 to eq. 13, v_p can be expressed with p_1 being the only variable, where under standard, non-choked conditions

$$v_p = \frac{C \cdot A_h \sqrt{2\ \rho_0\ p_1 \left(\frac{\gamma}{\gamma-1}\right)\left[\left(\frac{p_2}{p_1}\right)^{\frac{2}{\gamma}} - \left(\frac{p_2}{p_1}\right)^{\frac{\gamma+1}{\gamma}}\right]}}{p_1} \cdot \frac{RT}{M_r A_p} \tag{17}$$

$$v_p = A_h \cdot \sqrt{2 \cdot 1.293\,\mathrm{kg\,m^{-3}} \cdot p_1 \left(\frac{1.4}{1.4-1}\right)\left[\left(\frac{101\,325\,\mathrm{Pa}}{p_1}\right)^{\frac{2}{1.4}} - \left(\frac{101\,325\,\mathrm{Pa}}{p_1}\right)^{\frac{1.4+1}{1.4}}\right]} \cdot \frac{0.65 \cdot 8.3144\,\mathrm{J\,K^{-1}\,mol^{-1}} \cdot 300\,\mathrm{K}}{28.965\,\mathrm{kg\,mol^{-1}} \cdot A_p} \tag{18}$$

when $101\,325\,\mathrm{Pa} < p_1 < 191\,800\,\mathrm{Pa}$,

and under choked flow conditions,

$$v_p = \frac{A_h \sqrt{\gamma \rho_0 p_1 \left(\frac{2}{\gamma+1}\right)^{\frac{\gamma+1}{\gamma-1}}}}{p_1} \cdot \frac{RT}{M_r A_p} \tag{19}$$

$$v_p = \frac{A_h \sqrt{1.4 \cdot 1.293\,\mathrm{kg\,m^{-1}} p_1 \left(\frac{2}{1.4+1}\right)^{\frac{1.4+1}{1.4-1}}}}{p_1} \cdot \frac{8.3144\,\mathrm{J\,K^{-1}\,mol^{-1}} \cdot 300\,\mathrm{K}}{28.965\,\mathrm{kg\,mol^{-1}} \cdot A_p} \tag{20}$$

when $p_1 > 191\,800\,\mathrm{Pa}$.

For the rebound process, the air inside the chamber becomes downstream, p_2, and the atmosphere becomes upstream, p_2, giving

$$v_p = A_h \sqrt{2 \cdot 1.293\,\mathrm{kg\,m^{-3}} \cdot 101\,325\,\mathrm{Pa} \left(\frac{1.4}{1.4-1}\right)\left[\left(\frac{p_2}{101\,325\,\mathrm{Pa}}\right)^{\frac{2}{1.4}} - \left(\frac{p_2}{101\,325\,\mathrm{Pa}}\right)^{\frac{1.4+1}{1.4}}\right]} \cdot \frac{0.65 \cdot 8.3144\,\mathrm{J\,K^{-1}\,mol^{-1}} \cdot 300\,\mathrm{K}}{28.965\,\mathrm{kg\,mol^{-1}} \cdot A_p} \tag{21}$$

when $53\,530\,\mathrm{Pa} < p_2 < 101\,325\,\mathrm{Pa}$,

$$v_p = \frac{A_h \sqrt{1.4 \cdot 1.293\ \mathrm{kgm^{-1}} \cdot 101325\ \mathrm{Pa} \left(\frac{2}{1.4+1}\right)^{\frac{1.4+1}{1.4-1}}}}{101325\ \mathrm{Pa}} \cdot \frac{8.3144\ \mathrm{JK^{-1}mol^{-1}} \cdot 300\mathrm{K}}{28.965\ \mathrm{kgmol^{-1}} \cdot A_p} \tag{22}$$

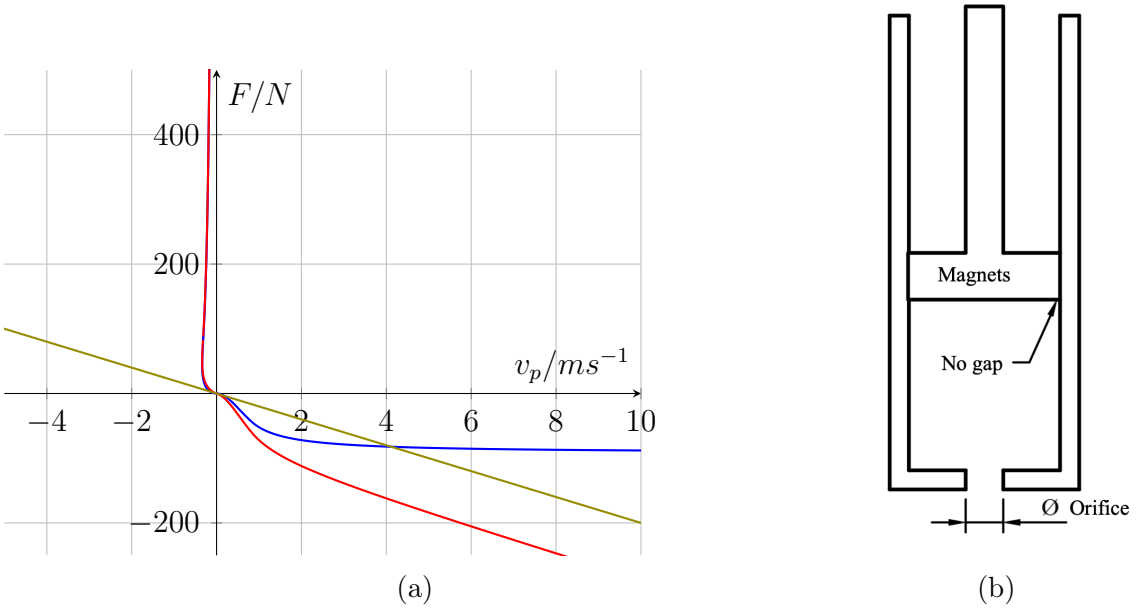

(a) (b)

Figure 5: (a): Red curve: theoretical overall damping curve of eddy current damping and air damping with constant air pressure inside the chamber. Isolated damping curves of eddy current and discharging air are in blue and olive, respectively. Parameters: piston ⌀34 mm and orifice ⌀2 mm, $p_{out} = 1\,\text{atm}$, coefficient of magnetic friction $= 20\,\text{N s m}^{-1}$. The direction of rebound is defined as positive. (b): The ideal piston with one air chamber.

when $p_2 < 53\,530\,\text{Pa}$.

The force on the piston can be calculated from

$$F = A_p \cdot p_{\text{chamber}} \tag{23}$$

The force on the piston and its velocity can be related by employing the pressure in the chamber as a parameter, forming a parametric equation plotted in fig. 5(a).

The graph suggests that the velocity of the piston cannot exceed a certain value during compression, where the mass discharge of air is maximised. This can be seen as a safety feature which prevents the piston from moving too fast and causing damage to the device. By adding one-way valves on the orifices of different sizes, the compression and the rebound curve can be isolated and modified as required. Be aware that this graph does not describe the device made because the minor air gaps between the piston and the shell do not behave as orifices and that the upper face of the piston also forms an enclosure with the upper part of the shell, where the pressure is less than 1 atm during compression and greater than 1 atm during rebound. Instead, this graph shows the damping curve of a device similar to fig. 5 (b). Overall, the damping force at low speed is mainly due to the resistance of airflow, while at high speeds, it is dominated by eddy currents.

5 Vibration transmissibility characteristics

To evaluate the vibration reduction ability of this system, a simple experiment is conducted. By rigidly connecting a stable source of vibration with known amplitude and frequency

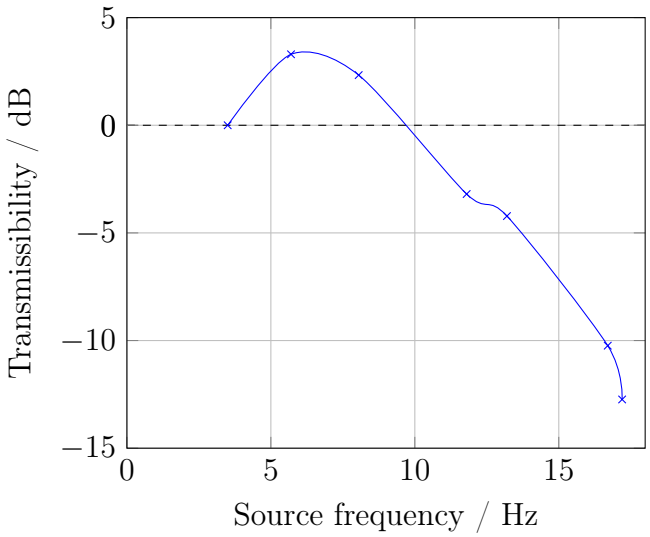

Figure 6: Vibration transmissibility of MSS at different frequencies. Mass of load = 2.5 kg. Source amplitude = 1.3 cm.

below the MSS, on the "Bottom" component, and measuring the vibration amplitude at the "Top" component, the amount of vibration reduced in decibels can be easily calculated using

$$L_A = 20 \cdot \log_{10}\left(\frac{A}{A_0}\right) \tag{24}$$

Where A is the detected amplitude at the top and A_0 is the source amplitude.

A stable source of vibration is generated using a hand drill connected to a "drill to jigsaw" accessory which converts the drill's rotational motion into a reciprocating motion with amplitude 1.3 cm. The MSS is rigidly connected to the conversion component via a 3D-printed piece. The entire setup is placed vertically, where 2.5 kg of load is placed on top of the MSS. The amplitudes of vibration are determined by measuring the displacement of the top with reference to a metre ruler in the footage recorded by a slow-motion camera. A magnet arrangement of "2-2" is used.

The source vibration frequence ranges from 3.5 Hz to 17.2 Hz. It is likely that this relatively small range of frequencies does not reveal the full performance of the MSS, e.g. unable to present peculiarity at certain high or low frequencies. However, the results obtained at this low range of frequencies demonstrate some of the key transmissibility characteristics.

As shown in fig. 6, the experimental natural frequency of the MSS is around 5.7 Hz, where the detected vibration is 3.3 dB greater than that of the source vibration. This again suggests that it is unsuitable for road vehicles, where the natural frequency is usually around 1 Hz to allow maximum comfort [13]. Similar to other common types of suspension systems, the vibration reduction ability increases significantly as the frequency increases beyond the natural frequency, reaching a satisfactory transmissibility of −12.7 dB at 17.2 Hz. Generally, the results obtained are adequate for a prototypical design, showcasing its high potential to be further developed.

6 Future Developments

The aerodynamic design (i.e. components involved in air damping) of MSS is functionally vulnerable compared to the other components, considering its sensitivity to manufacturing accuracy. The assumption that the pressure in the chamber remains a constant made in section 4.1 is unrealistic in real-world situations where the air mass varies non-linearly during operation. However, this assumption allows much simpler calculations and gives a clue to the general characteristics of the damping curve. After all, though air damping is functionally effective in this suspension system by making up for the insufficient eddy current damping force, it sets constraints to its use in a greater range of environments, e.g. under water or in vacuum, which was what this design originally aimed for. The air damping mechanism may be eliminated if the effect of eddy current damping is improved by, for example, adding magnets on the side of the piston that moves along with the piston and generates additional resistive forces without increasing the repulsion.

Further investigations can be made by replacing the permanent magnets with electromagnets, allowing the suspension system's behaviour to be adjusted. This might be an effective active suspension design where the spring force can be adjusted near-instantly during work without modifying any mechanical structure. With this design, it might be possible to integrate the damping module into the spring as the force of the spring can be controlled with a true non-reliance on damping fluid or any separate mechanical structure for damping. This allows specific applications in vacuum environments where energy dissipation is a huge issue because the internal energy of the device cannot be transferred to the external environment apart from via thermal radiation.

7 Conclusion

Overall, the proposed Magnetic Suspension System is passive and progressive. Since this design does not have any specified uses and, unfortunately, specialised testing devices are not available, this prototype did not undergo any dynamic or static tests apart from the ones mentioned in this article. Its expected advantages include a long life span, convenient maintenance, compactness, and the fact that it does not require any component to be sealed, making it suitable for some of the less common applications where longevity, reliability and size are of importance, for example, in the aviation industry. However, compared to other existing alternatives, it is extremely progressive and thus can be uncommon among daily uses, for example, in most vehicle suspensions where a large and linear travel is needed to allow comfort. It is also worth mentioning that as a result of using strong magnets, nearby electronics might malfunction and ferrous items are prone to be attracted.

Acknowledgement

The author thanks Oleksandr Korpanyuk for 3D printing the components used for testing and experiments. The author appreciates Byron College and Dr. Dario Papavassiliou for providing equipment for experiments and guidance.

References

[1] Henri Nielens and Thierry Lejeune. "Bicycle shock absorption systems and energy expended by the cyclist". In: *Sports Medicine* 34.2 (Jan. 1, 2004), pp. 71–80. DOI: 10.2165/00007256-200434020-00001.

[2] M. Menzel et al. "The Design, Verification, and Performance of the James Webb Space Telescope". In: *Publications of the Astronomical Society of the Pacific* 135.1047 (June 6, 2023), p. 058002. DOI: 10.1088/1538-3873/acbb9f. URL: https://dx.doi.org/10.1088/1538-3873/acbb9f.

[3] Automated Industrial Motion. *ALL ABOUT SPRINGS*. Oct. 2019. URL: https://aimcoil.com/new-resource-for-manufacturers-all-about-springs-ebook/.

[4] K and J Magnetics. *Magnet Strength Calculator*. URL: https://www.kjmagnetics.com/magnet-strength-calculator.asp.

[5] Bruce Lin. *Coil vs Air Shocks: Pros and Cons of MTB Shocks*. May 11, 2022. URL: https://www.theproscloset.com/blogs/news/mountain-bike-shocks?srsltid=AfmBOoo246P20ES23KDKEhqf_G-qnvAqI-0LkbddAq9FVOBQ8eXoveHy.

[6] Stanford Magnets. *Maximum Operating Temperature VS. Curie Temperature | Stanford Magnets*. URL: https://www.stanfordmagnets.com/maximum-operating-temperature-vs-curie-temperature.html.

[7] Ke Zhang. "Magnetic vibration reducing method and vibration dampener". CN101067434A. Nov. 7, 2007.

[8] Honeybee Robotics. *Eddy Current Dampers*. URL: https://www.honeybeerobotics.com/products/eddy-current-dampers.

[9] Wenbin Yu and Guolai Yang. "Eddy current damper capable of collecting electric energy". In: *Vibroengineering PROCEDIA* 33 (Oct. 19, 2020), pp. 28–33. DOI: 10.21595/vp.2020.21672.

[10] Pasquale Onorato and Anna De Ambrosis. "Magnetic damping: Integrating experimental and theoretical analysis". In: *American Journal of Physics* 80.1 (Dec. 2011), pp. 27–35. DOI: 10.1119/1.3647997.

[11] Tamer M. Abdo et al. "Characteristics and analysis of an Eddy Current Shock absorber damper using finite element analysis". In: vol. 8. 4. Nov. 19, 2019, p. 77. DOI: 10.3390/act8040077.

[12] Federal Emergency Management Agency, U.S. Department of Transportation, and U.S. Environmental Protection Agency. *B.3 Gas Discharge From a Tank*. 1989, B–4. URL: https://nepis.epa.gov/Exe/ZyPURL.cgi?Dockey=10003MK5.txt.

[13] Sanjay Sharma et al. "Modal and frequency response characteristics of vehicle suspension system using full car model". In: *IOP Conference Series Materials Science and Engineering* 810.1 (Mar. 1, 2020), p. 012056. DOI: 10.1088/1757-899x/810/1/012056.

Appendix

Table I. Full experimental data of the magnetic repulsion force vs. distance between magnets

Magnets Arrangement	Distance/cm	True distance/cm	Force/gf
⌀30mm 1-1	2.8	3.3	150
	2.2	2.7	279
	1.8	2.3	374
	1.5	2.0	593
	1.0	1.5	1265
	0.7	1.2	2245
	0.5	1.0	3074
⌀30mm 1-2	3.0	3.8	219
	2.5	3.3	329
	2.0	2.8	503
	1.5	2.3	917
	1.2	2.0	1302
	1.0	1.8	2070
	0.6	1.4	4070
⌀30mm 2-2	2.5	3.5	765
	1.8	2.8	1223
	1.4	2.4	1959
	1.0	2.0	2970
	0.7	1.7	4310
	0.5	1.5	5370
⌀30mm 2-3	3.5	4.5	418
	3.0	4.0	680
	2.0	3.0	1780
	1.4	2.4	2180
	1.0	2.0	3440
	0.7	1.7	4550
⌀30mm 3-3	3.5	5.0	522
	3.0	4.5	716
	2.5	4.0	1029
	2.0	3.5	1530
	1.5	3.0	2359
	1.0	2.5	3804
	0.7	2.2	5100
⌀30mm 2-4	3.0	4.5	650
	2.5	4.0	960
	2.0	3.5	1470
	1.5	3.0	2330

Continued on next page

Table 1 Continued from previous page

Magnets Arrangement	Distance/cm	True distance/cm	Force/gf
	1.0	2.5	3577
	0.7	2.2	5355
⌀30mm 3-4	3.5	5.3	630
	3.0	4.8	830
	2.5	4.3	1280
	2.0	3.8	1805
	1.5	3.3	2638
	1.0	2.8	4554
	0.7	2.5	6250
⌀30mm 4-4	3.5	5.5	700
	3.0	5.0	1010
	2.5	4.5	1364
	2.0	4.0	1970
	1.5	3.5	2950
	1.2	3.2	4333
	0.8	2.8	6310
⌀40mm 1-1	8.2	8.7	100
	6.2	6.7	200
	4.2	4.7	1450
	3.0	3.5	3200
	2.3	2.8	5700
	1.9	2.4	10200
	1.6	2.1	15200

Concluded

II. Technical drawing of the Magnetic Suspension System prototype

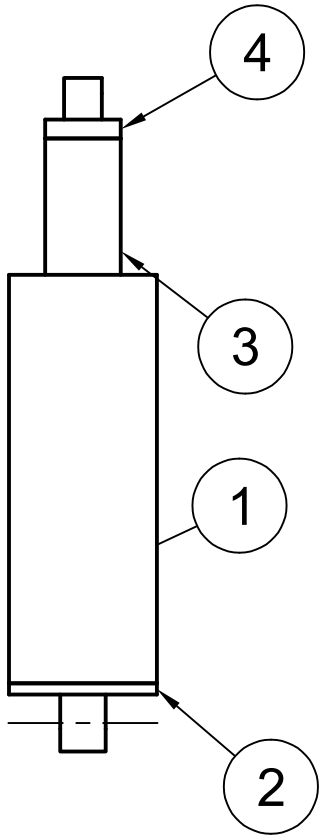

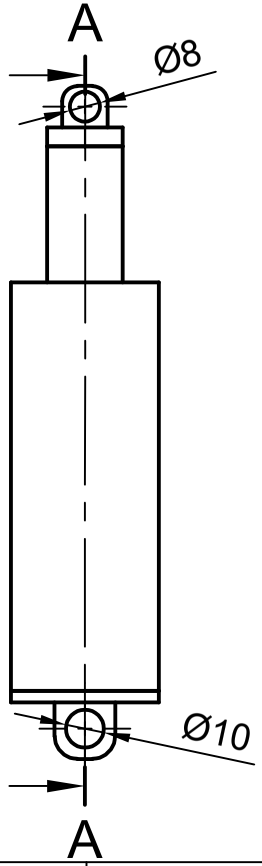

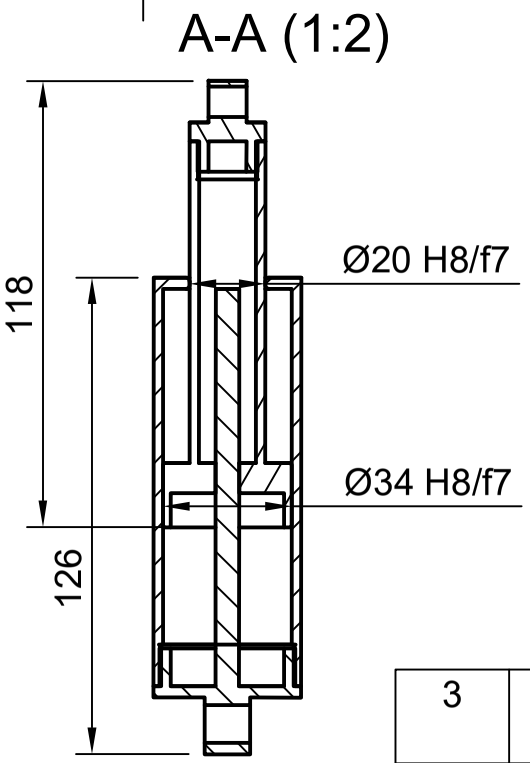

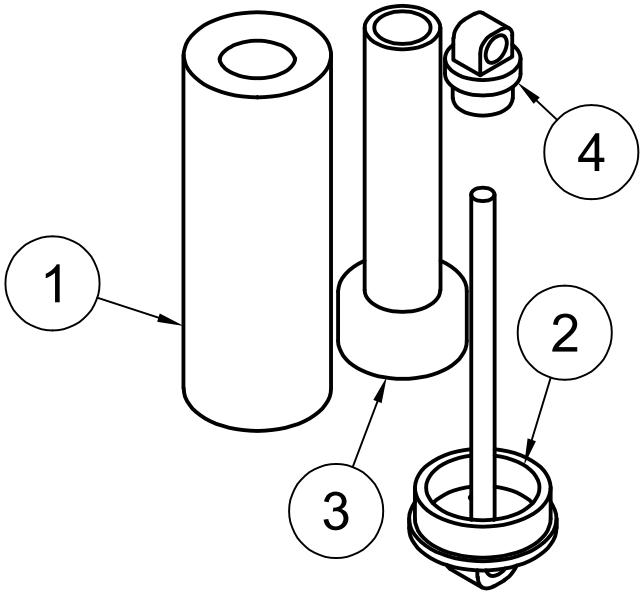

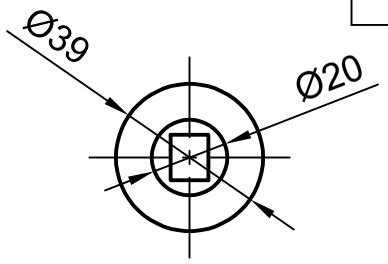

Item	Qty	Part Name	Material
4	1	Top	Aluminum 6061
3	1	Piston	Aluminum 6061
2	1	Bottom	Aluminum 6061
1	1	Shell	Aluminum 6061

Parts List

Dept.	Technical reference	Created by: Zimo Chen	Approved by
		Document type: Assembly Drawing (1:2)	Document status
		Title: **Magnetic Suspension**	DWG No.
			Rev. / Date of issue: 03/12/2024 / Sheet: 0/4

B (3:1)

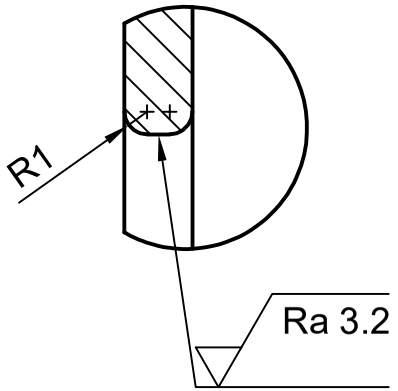

A-A (1:1)

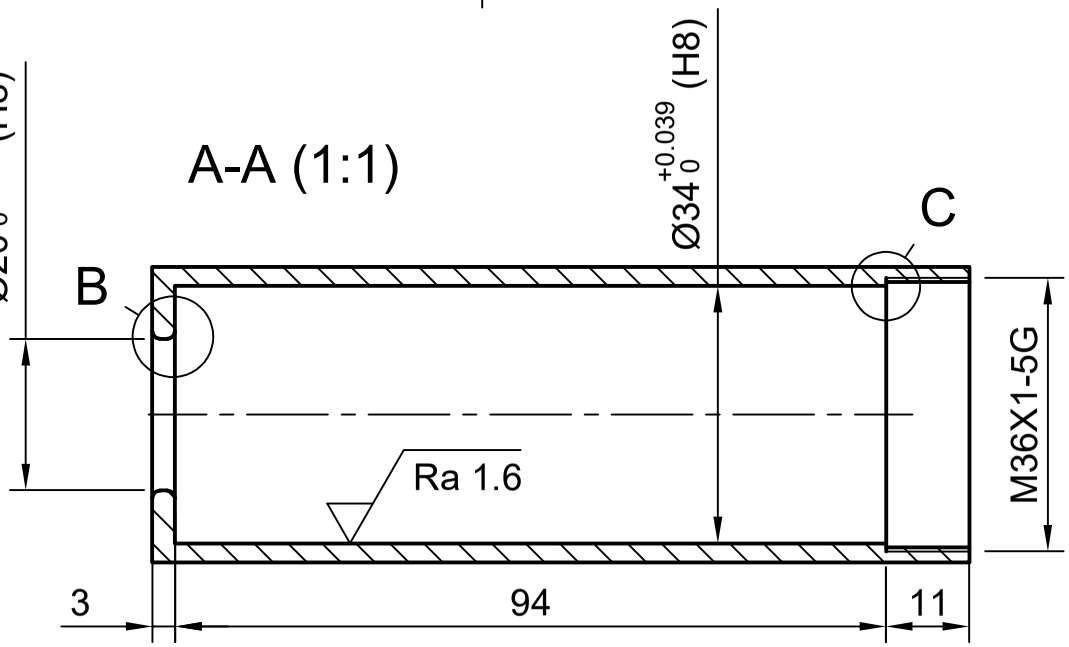

C (3:1)

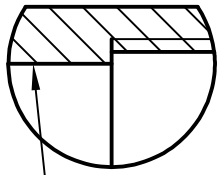

Diameter of the smooth part is slightly smaller than the minor diameter of the threads.

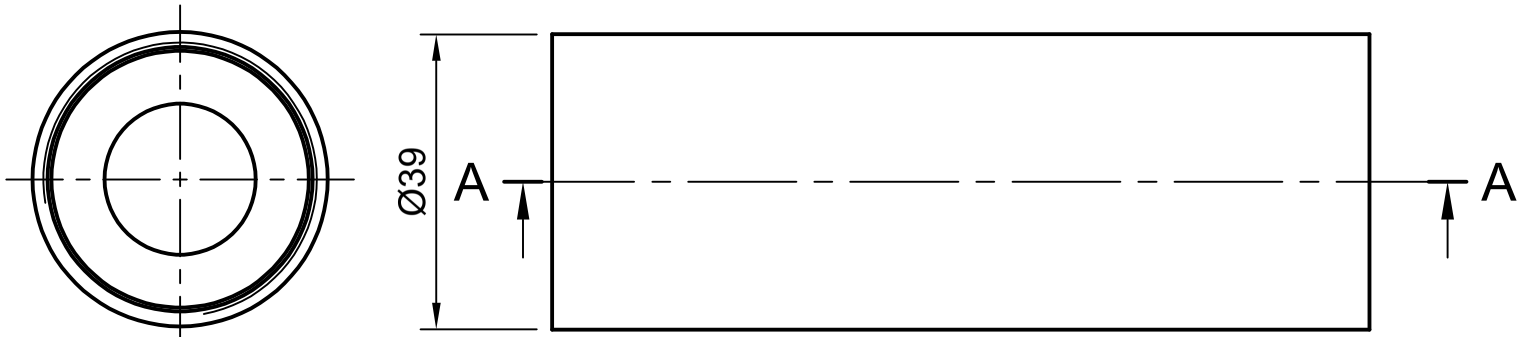

Dept.	Technical reference	Created by	Approved by
		Zimo Chen	
		Document type: Part Drawing (1:1)	Document status
		Title: Magnetic Suspension Shell Component number:1	DWG No.
			Rev. / Date of issue: 03/12/2024 / Sheet: 1/4

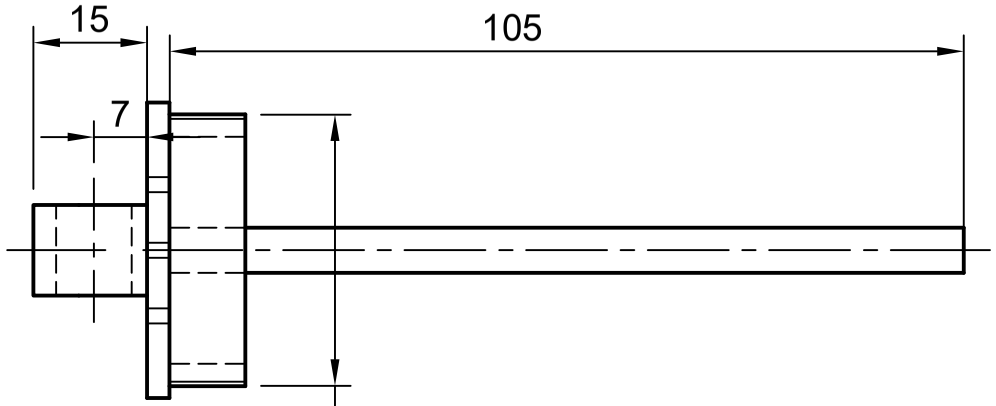

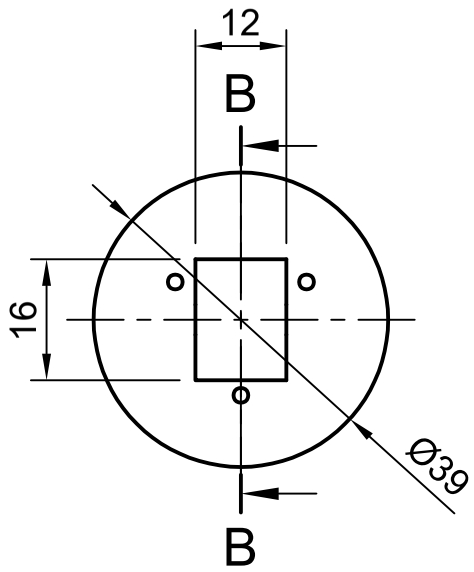

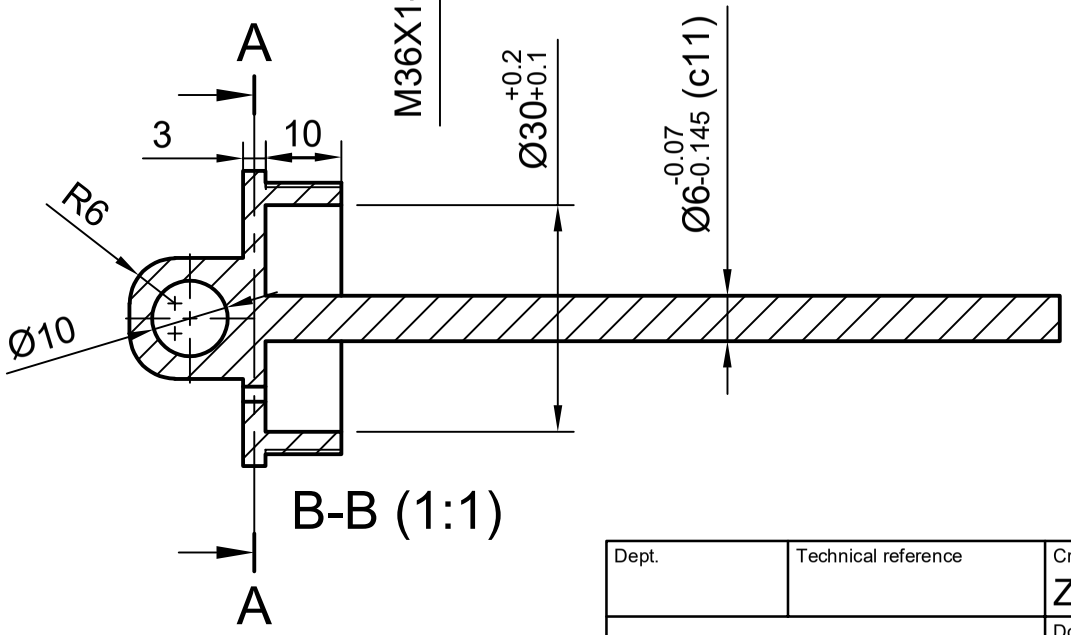

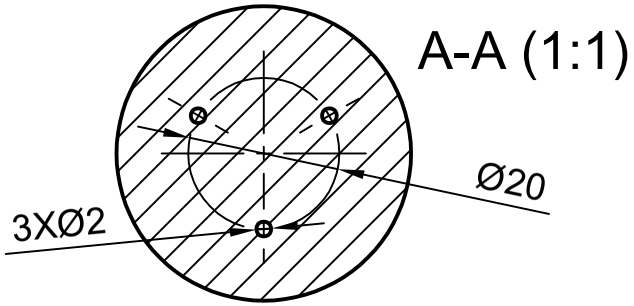

Dept.	Technical reference	Created by	Approved by	
		Zimo Chen		
		Document type	Document status	
		Part Drawing(1:1)		
		Title	DWG No.	
		Magnetic Suspension Bottom Component number: 2		
			Rev.	Date of issue: 03/12/2024
				Sheet: 2/4

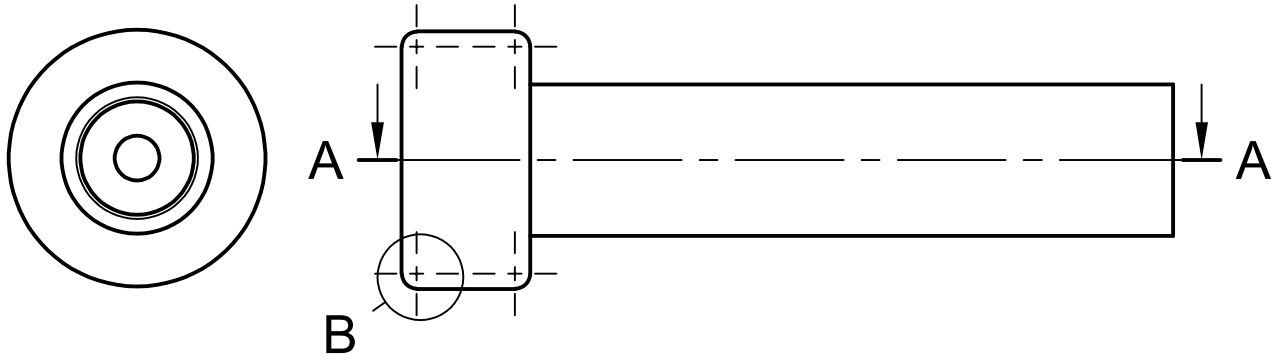

B (3:1)

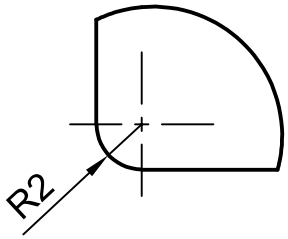

A-A (1:1)

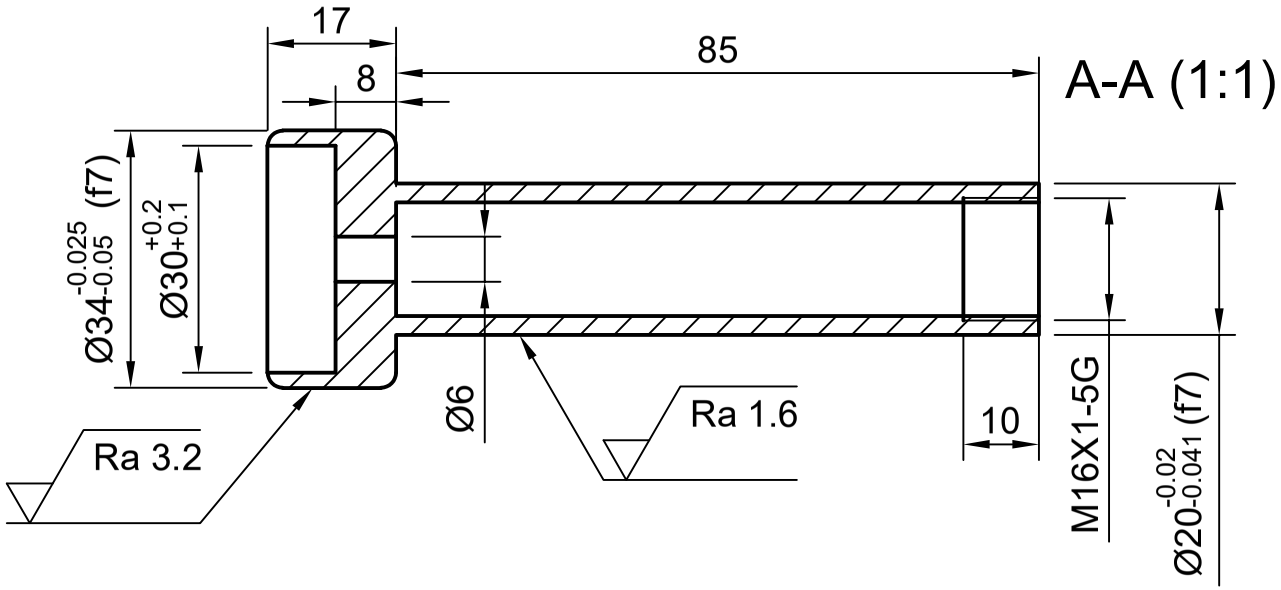

Dept.	Technical reference	Created by	Approved by	
		Zimo Chen		
		Document type	Document status	
		Part Drawing(1:1)		
		Title	DWG No.	
		Magnetic Suspension Piston Component number: 3		
			Rev.	Date of issue: 03/12/2024 — Sheet: 3/4

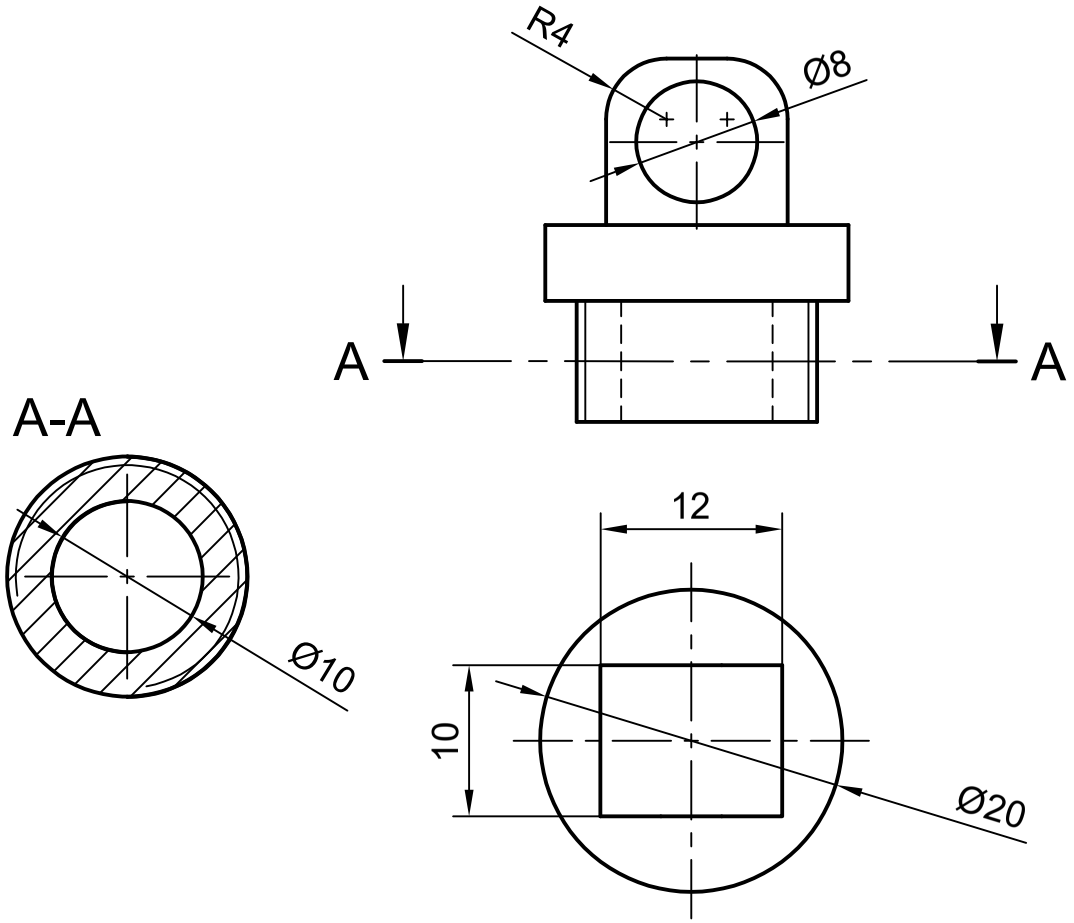

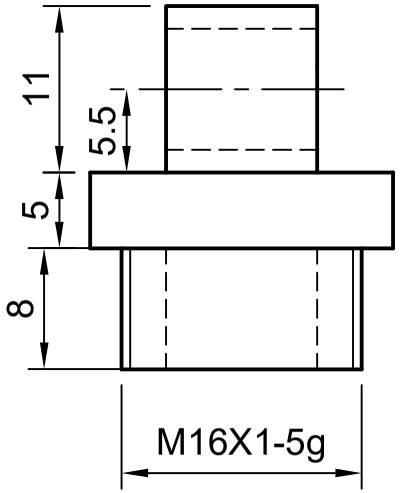

Dept.	Technical reference	Created by Zimo Chen	Approved by	
		Document type Part Drawing(2:1)	Document status	
		Title **Magnetic Suspension Top** **Component number: 4**	DWG No.	
			Rev.	Date of issue 03/12/2024	Sheet 4/4